Journal of Alloys and Compounds 884 (2021) 161114

Contents lists available at ScienceDirect

Journal of Alloys and Compounds

journal homepage: www.elsevier.com/locate/jalcom

Thermodynamic evidence of the ferroelectric Berry phase in europium-based ferrobismuthite $Eu_2Bi_2Fe_4O_{12}$

A.V. Gil Rebaza[a], C.E. Deluque Toro[b], H.H. Medina Chanduví[a], D.A. Landínez Téllez[c,d], J. Roa-Rojas[c,*]

[a] Depto. de Física, Facultad de Ciencias Exactas – UNLP, Instituto de Física La Plata – IFLP, CONICET-CCT La Plata, (1900), La Plata, Argentina
[b] Grupo de Nuevos Materiales, Facultad de Ingeniería, Universidad del Magdalena, Santa Marta, Colombia
[c] Grupo de Física de Nuevos Materiales, Departamento de Física, Universidad Nacional de Colombia, 111321 Bogotá D.C., Colombia
[d] Grupo de Estudios de Materiales GEMA, Departamento de Física, Universidad Nacional de Colombia, 111321 Bogotá D.C., Colombia

ARTICLE INFO

Article history:
Received 1 May 2021
Received in revised form 2 July 2021
Accepted 8 July 2021
Available online 10 July 2021

Keywords:
Complex perovskite
Electronic structure
Thermophysical properties

ABSTRACT

The possible low temperature biferroic feature of $Eu_2Bi_2Fe_4O_{12}$ complex perovskites was recently reported. The aim of this work is to present a theoretical study of the structural, magnetic, electronic and ferroelectric properties of this material. Several energy minimization processes were performed for three types of cationic distributions, different angles of rotation, octahedral inclination, and some kinds of magnetic ordering. The results reveal that the most stable crystallographic arrangement corresponds to an intercalated distribution of the Eu^{3+} and Bi^{3+} cations between the FeO_6 octahedra. Similarly, energy is minimized for rotations and octahedral inclinations corresponding to angles $\theta_e = 12.86°$ and $\phi_e = 13.32°$, respectively. With respect to the distribution of magnetic moments, the results reveal that a G-type antiferromagnetic configuration is the most energetically favorable. The electronic structure is studied from ab initio calculations following the formalism of density functional theory and the pseudopotential plane wave method. In this formalism, the exchange and correlation mechanisms are described by means of the generalized gradient approach (GGA + U), considering spin polarization. The ferroelectric characteristic is analysed by determining ferroelectric polarization based on the calculation of the Berry phase. The theoretical results obtained are consistent with the experimental reports, which is why the $Eu_2Bi_2Fe_4O_{12}$ material is expected to exhibit biferroic behavior at low temperatures, because the Berry phase introduces hybridizations between the 3d-Fe and 2p-O states that favor the occurrence of Dzyaloshinskii-Moriya interactions, which facilitate the occurrence of ferroelectricity coexisting with weak ferromagnetism. An extensive study of the thermodynamic properties in the presence and absence of the Berry phase is undertaken by means of the Debye quasi harmonic model. The specific heat difference with and without the Berry phase reveals the occurrence of a ferroelectric transition at T = 113 K without the application of external pressure. When the applied pressure is incremented, a systematic increase in the transition temperature is observed due to the reduction of overlap between the 3d-Fe orbitals and the 2p-O orbitals in the compressed octahedra of perovskite.

1. Introduction

In recent decades, considerable efforts have been undertaken in the search for new physical properties, as well as in the optimization of those already discovered in perovskite-type materials, with a view to applications in various technological and industrial fields as sophisticated as spintronics [1–3]. In fact, the ideal formula ABO_3 and the structure of perovskite ceramics are well known, as well as the versatile possibility of crystallographic modification that allows the variability of their physical properties [4]. Among all the simple perovskites reported, bismuth ferrite $BiFeO_3$ has received special attention due to its properties first reported in 1957 with uncertainty regarding the type of magnetic arrangement [5]. This material crystallizes in a polar rhombohedral structure belonging to the $R\bar{3}c$ space group (# 67) [6], with evidence of ferroelectric hysteresis and ferroelastic monodomains [7]. The axis of electrical polarization was determined to be the rhombohedral c-axis [8]. Approximately fifty years after its first report, it was established that

* Corresponding author.
E-mail address: jroar@unal.edu.co (J. Roa-Rojas).

https://doi.org/10.1016/j.jallcom.2021.161114
0925-8388/

the material presents G-type antiferromagnetic ordering with a modulated cycloidal spin structure below a Néel temperature of 643 K [9]. Meanwhile, the cycloid spin structure seems to inhibit the macroscopic magnetic response, making direct observation of the linear magnetoelectric effect difficult [10], but still at room temperature, it is possible to determine the occurrence of weak ferromagnetism, whose Curie temperature has been determined to be 1043 K [11]. On the other hand, $RFeO_3$ rare earth orthoferrites are simple perovskites that crystallize in orthorhombic structure, Pbnm space group (# 62), with the Fe^{3+} cation in octahedral coordination centered around the 6 closest neighbouring oxygen and minimum tilting of the octahedral axes relative to the *c* crystallographic axis [12]. The crystalline structure turns out to be the same for rare earths (lanthanides), so that the R^{3+} cation forms the common vertex of two adjacent octahedra, mediating the super exchange interaction between two Fe^{3+} cations [13]. On the other hand, the magnetic ordering that takes place in the material has been classified as a G-type antiferromagnetic [14], with a weak ferromagnetic contribution [15], and the particularity that the Néel temperature value shows a direct dependence on the ionic radii of the rare earth, evidencing a minimum of 625 K for Lu and a maximum of 743 K for La [16]. In the specific case of R = Eu, changes in hyperfine interaction parameters have been reported when samples of $EuFeO_3$ are subjected to hydrostatic pressures between 45 and 52 GPa, which have been attributed to strong distortions in Fe-O_6 octahedra as a result of the small ionic radius of the Eu^{3+} cation [17]. In addition, due to its centrosymmetric structure at room temperature, this material exhibits ferromagnetism and antiferromagnetic ordering-induced ferroelectricity caused by non-equivalent spins [18]. In the experimental search for a complex perovskite from the two simple perovskites $BiFeO_3$ and $EuFeO_3$, the synthesis and study of the structural, electrical, and magnetic properties of the $EuBiFe_2O_6$ material were investigated. [19]. The corresponding structure of this material belongs to the family known as complex perovskites such as $AA'B_2O_6$ [20], with A and A′ representing rare earths or alkaline earths and B transition metals and even rare earths. [21]. It can be inferred that the characteristic properties of the material depend strongly on the ionic radius and the electronic configuration of the A, A′ and B cations that constitute the material, as well as the chemical bonds, the exchange mechanisms and the effects of coupling between these, which give rise to structural spatial groups and specific octahedral distortions [22,23]. The $AA'B_2O_6$ formula for this double perovskite is usually written as $A_2A'_2B_4O_{12}$ because of the atomic occupation in the structure, for which the material has been reported as $Eu_2Bi_2Fe_4O_{12}$ [19]. It was observed that the material behaves like a weak ferromagnetic semiconductor at room temperature, with evidence of a possible ferroelectric state at temperatures below 112.8 K, where magnetoelectric behavior would take place [19]. To theoretically establish the possibility of the occurrence of ferroelectricity at temperatures close to T = 0 K, in this original work, we determined the configuration of magnetic ordering of lower energy, subsequently calculating the electronic structure and the charge density of the system through density functional theory (DFT), as well as the Berry phase for the establishment of electrical polarization effects for the $Eu_2Bi_2Fe_4O_{12}$ complex perovskite. The Berry phase can be understood as the polarization difference (ΔP) between two structural configurations given in the cell of the same crystal: one without distortion and the other containing a structural distortion that leads to the formation of a dipole moment in the cell. In other words, ΔP can be obtained using a model whose starting point is the electronic wave functions of the ground state of the crystal in the two states, without distortion and with distortion [24]. The calculation of ΔP is carried out through the introduction of a dimensionless parameter λ, which constitutes a measure of the amplitude of the ferroelectric distortion between the center-symmetric ideal structure ($\lambda = 0$) and the ferroelectric polar structure ($\lambda = 1$), assuming the occurrence of a continuous adiabatic transformation where the internal strain is scaled with the parameter λ in the interval $0 < \lambda < 1$ [25]. In recent years, predictions of thermophysical behavior have been made in perovskite-like materials that allow studying the dependence of energy requirements on temperature [26,27]. The formalism that facilitates this study of equilibrium properties is based on the so-called quasi-harmonic Debye model [28], which allows the calculation both under consideration and in the absence of the Berry phase, from which it is expected to obtain information conducive to the eventual corroboration of the occurrence of magnetoelectric coupling at low temperatures in the $Eu_2Bi_2Fe_4O_{12}$ material.

2. Computational details

Ab initio spin-polarized calculations have been performed in the framework of the DFT [29], where the Kohn-Sham self-consistent equations were solved using the plane-wave and pseudopotential method implemented in the Quantum Espresso code [30]. The exchange-correlation contribution was described in the context of the Perdew-Burke-Ernzerhof parametrization into the General Gradient Approximation (GGA-PBE) [31]. Furthermore, for a better description of the electronic band structure and magnetic properties, we considered the addition of the Hubbard U term (DFT + U) in the self-interaction correction scheme, with a value U for the *3d-Fe* (U = 8.0 eV) and orbitals being determined through the linear response approach [32,33]. To describe the ionic cores of the atoms, we used Projected Augmented Wave (PAW) pseudopotentials from the Standard Solid State Pseudopotential library (SSSP) [34]. After the convergence study, the kinetic energy cut off for the wave function and charge density were set to 80 Ry and 800 Ry, respectively. The reciprocal k-space was described by a dense mesh grid of 9 × 9 × 9 k-points in the irreducible Brillouin zone, according to the Monkhorst-Pack scheme [35]. Calculation of the spontaneous polarization was performed using Berry phase calculation based on the modern theory of polarization [36,37]. Considering that ΔP represents the macroscopic polarization between two different states of the same solid, calculations of the density of states (DOS) for undistorted and distorted structures were carried out separately [38]. The calculation of the thermodynamic properties for both the deformed structure and the undeformed lattice, i.e., considering and without considering the Berry phase, is carried out following the quasi-harmonic Debye model [39]. In the model, under the application of external changes in pressure and temperature, the macroscopically evident thermodynamic properties are directly associated with the microscopic dynamics of the atoms within the material. Because the collective vibrations of the crystalline cells of solid materials take place in the form of discrete energy quasiparticles, called phonons, it is possible to study the fundamental excitations associated with these thermophysical properties. Phonons play a particularly important role in insulating and semiconducting materials, making direct contributions to properties such as specific heat and thermal expansion as a function of temperature. Thus, crystalline vibrations are expected to exhibit a harmonic character for temperature values below the Debye temperature of the solid. In this work, the quasi-harmonic Debye model is applied as part of the study of atomic dynamics at relatively high temperatures.

3. Results and discussion

Based on the experimental result previously reported [19], calculations were made considering the Pnma space group (# 62). Since the electronic properties of the material strongly depend on the distribution of ions in its crystalline structure, it is necessary to establish the type of arrangement of the Eu^{3+} and Bi^{3+} cations in the unit cell corresponding to the stoichiometry $Eu_2Bi_2Fe_4O_{12}$. For this

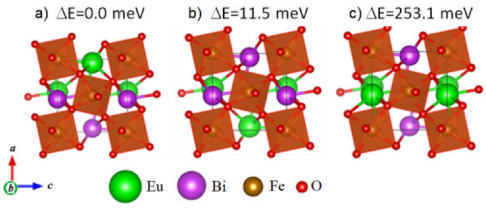

Fig. 1. Cationic arrangements considered in the calculation of energy minimization (a) superstructure with alternating arrangement of the Eu^{3+} and Bi^{3+} cations always alternating in the three crystallographic directions, (b) Alternating inverse along the crystallographic *a*-axis with respect to figures (a), and (c) alternate planes along the *c*-axis.

purpose, the four types of cationic ordering shown in Fig. 1 are considered in an energy minimization process. The most stable configuration corresponds to the case of a superstructure type arrangement, in which all the cations of Eu^{3+} and Bi^{3+} are sited in an always alternating arrangement along the three crystallographic axes. This result is consistent with experimental reports, where the simultaneous occurrence of diffractor planes (111), (222), (131), (151), (331), (011), (101), (110), (022), (202) and (220) are a kind of fingerprint that characterizes this type of arrangement [40].

In the previous process, Fe^{3+} cations remained rigid and octahedrally coordinated with three pairs of oxygen, but it is relevant to consider the distortion of the octahedra associated with the Pnma spatial group, in which they present tilting $a^+b^-b^-$ (*in phase* with respect to sub axis *a* of the sub cell in which the octahedra are circumscribed and *out of phase* in the other axes) [41]. For this purpose, a slight structural deformation of rotation around the vertical octahedral axis is performed, as shown in Fig. 2, calculating the total energy of the compound, and repeating the calculation for several small rotation angles θ. Fig. 2(a) exemplifies the dependence of total energy on the variation in the rotation angle, reaching the minimum energy value for theta $\theta_e = 12.86°$. Subsequently, an inclination of the plane formed by the four basal atoms of oxygen and iron is applied through an angle ϕ, as shown in Fig. 2(b), where the calculation of energy is presented as a function of the angle ϕ. As seen in the picture, the minimum energy value is set for $\phi_e = 13.32°$. This structural configuration is in good agreement with the analysis of experimental data obtained by XRD measurements [19].

To evaluate the most likely type of magnetic arrangement, a configuration of ferromagnetic (FM) couplings and three different configurations of antiferromagnetic (AF) types A, C, and G were studied, as shown in Fig. 3. From the energy minimization procedures, it is obtained that the lowest energy takes place for the G-type AF configuration, for which zero energy value is established, with energies 1233.0 meV (FM), 728.3 meV (A-type AF), and 300.6 meV (C-type AF). The absolute value of the effective magnetic moment calculated for the Fe atom in the electronic density is 4.0 μ_B. This result differs substantially from that expected from the Hund rules, since the latter is a very ideal model that does not consider hybridizations between orbitals so that electrons are not shared but remain restricted within their orbitals [42]. Meanwhile, the result is consistent with the experimental report that for this material suggests a weakly FM behavior at room temperature with a magnetic reorientation below T = 112.8 K, probably performed with an AF response at very low temperatures, accompanied by magnetoelectric coupling that manifests itself in a drastic change in the thermostimulated depolarization current [19].

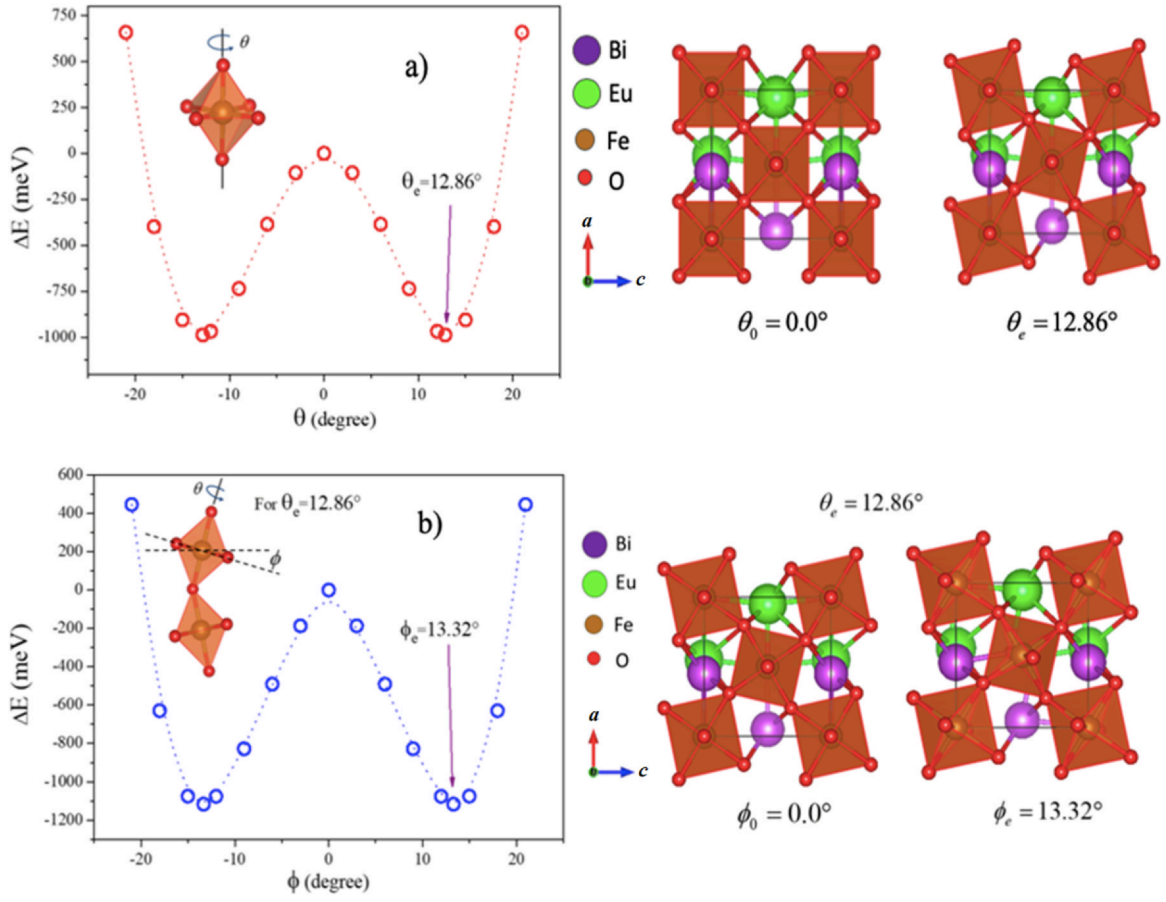

Fig. 2. Octahedral distortion of the $Eu_2Bi_2Fe_4O_{12}$ complex perovskite as a rotation in θ around the vertical axis (a) and tilting of the ϕ angle (b). The corresponding structures are shown to the right of figures (a) and (b).

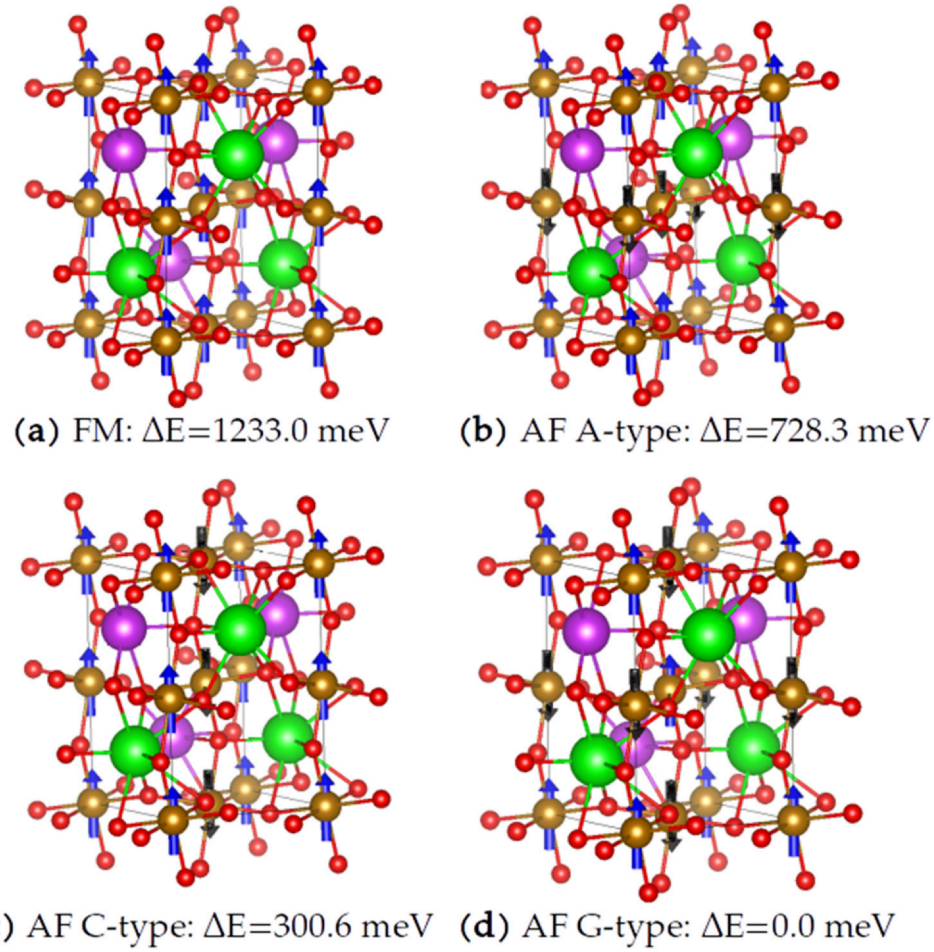

Fig. 3. Minimized energies of the $Eu_2Bi_2Fe_4O_{12}$ double perovskite for the magnetic configurations: (a) FM, (b) A-type AF, (c) C-type AF, and (d) G-type AF.

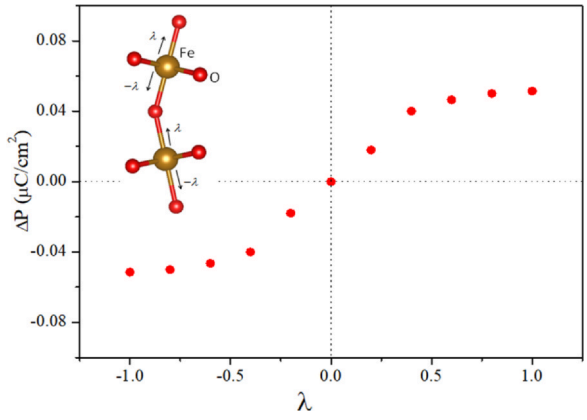

Fig. 4. Ferroelectric feature of the polarization curve calculated for $Eu_2Bi_2Fe_4O_{12}$ from the application of Berry's phase.

The macroscopic polarization of the material is calculated as a Berry phase of Bloch's electronic wave functions at zero temperature and in the absence of an applied electric field, that is, as a spontaneous polarization in a ferroelectric material [24,25]. Because there is no external electric field, the polarization process must be caused by lattice dynamics and based on a structural and magnetic ground state configuration. The previous experimental work for the $Eu_2Bi_2Fe_4O_{12}$ complex perovskite foresees the occurrence of an abrupt change in the thermostimulated depolarization current at T = 112.8 K [19], so it would be expected that this change would be associated with microscopic displacements of Fe cations from their symmetry sites in FeO_6 octahedra. The distortion should determine the preferred polarity of the axis, giving rise to spontaneous polarization. Thus, for the determination of the polarization of the compound, the structural and magnetic configuration of the fundamental state described above has been used, making several self-tests for different infinitesimal displacements of the parameter λ of the Fe atom, defined along the main axis of the octahedron, and for two opposite directions, as shown in Fig. 4. For each displacement, the ionic and electronic contributions of the polarization were calculated, obtaining the variation of the total polarization (ΔP) as a function of the λ displacement, as seen in Fig. 4. The resulting polarization curve exhibits a characteristic hysteretic behavior of ferroelectric materials with a polarization saturation value of 0.05 μC/cm^2.

The results of the state density calculations for the complex perovskite $Eu_2Bi_2Fe_4O_{12}$ are presented in Fig. 5, in which the reference energy E = 0 eV corresponds to the Fermi energy (E_F) of the electron system. The left picture corresponds to total and partial DOS without distortion and the right to total and partial DOS including distortion. The positive regimes of DOS represent the spin-up polarization, and the negative regimes represent the spin-down configuration. In the total DOS represented in Fig. 5(a), it is possible to observe the occurrence of a band gap around the Fermi level, which has a value E_g = 1.65 eV, allowing the classification of the material as a semiconductor type. This value is lower than that reported from experimental measurements at room temperature (E_g = 2.65 eV) [19]. The difference between the theoretical and experimental values takes place because the calculations are made for T = 0 K and because

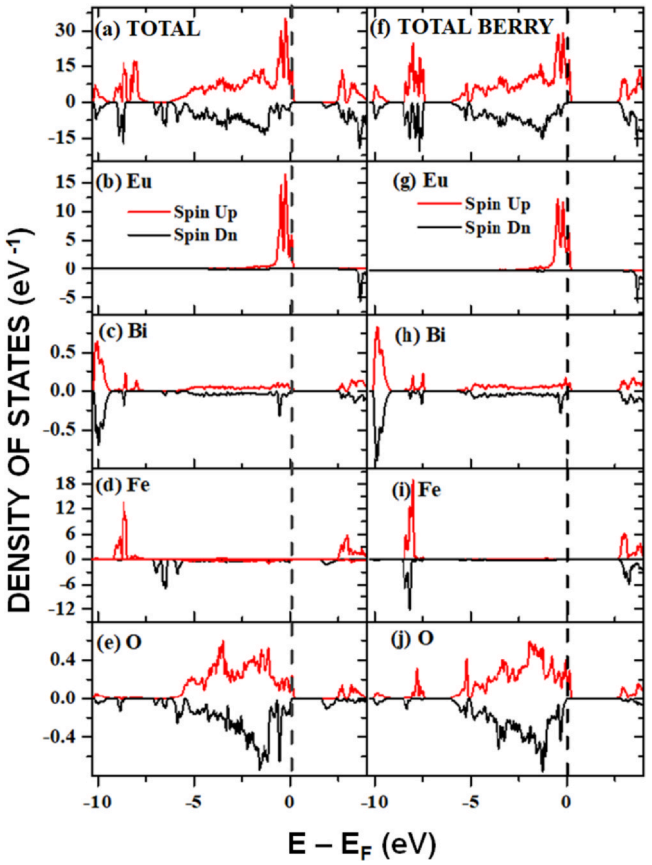

Fig. 5. Total DOS for the $Eu_2Bi_2Fe_4O_{12}$ undistorted structure is presented in (a) and (b), (c), (d) and (e) are the partial DOS of Eu, Bi, Fe and O, respectively. Total DOS for the distorted structure is exemplified in (f) and partial DOS for Eu, Bi, Fe and O are shown in (g), (h), (i), and (j), respectively.

the approximations that are considered there can lead to a slight underestimation of the gap. This is notable in Fig. 5(b) that the electronic orbitals of Eu make important contributions to the DOS in the valence band for spin-up polarization but do not have relevance in the conduction band close to the Fermi level. This contribution is mainly due to the *4f*-Eu orbitals. Likewise, a small participation of the *6s-Bi* orbitals is observed in Fig. 5(c) in the vicinity of E_F in the valence band and of the *5f-Bi* states in the conduction band, above E = 2.01 eV, for both up and down spin configurations. From Fig. 5(d), the insignificance of the 4s-*Fe* and *3p-Fe* orbitals close to the Fermi level in the valence band can be established, where asymmetric states between −5.43 and −7.23 eV are clearly observed for the spin down orientation and between −8.33 and −9.33 eV for the spin up direction. In the conduction band, the prominent role depends on the *3d-Fe* orbitals in the conduction band for the spin down orientation starting at E = 1.65 eV, while for the spin up configuration, these orbitals contain available states above E = 2.50 eV.

The small participation of the *2p-O* orbitals in the valence band is observed in Fig. 5(e) for the two spin configurations, with strong hybridizations due to Eu-O cuboctahedral coordination and weak cuboctahedral *Bi-O* and octahedral Fe-O hybridizations. In the conduction band, just above the band gap, between 1.65 and 2.53 eV, the hybridizations between the *2p-O* and *3d-Fe* states in the *Fe-O_6* octahedra have marked relevance for the spin down channel, which are primarily responsible for the band gap of the system.

Fig. 5(f) shows the total DOS for the distorted system. The first notable result is the expansion of the band gap, which reaches an E_g = 2.75 eV value. As seen in Fig. 5(g) and (h), for both up and down spin channels, all Eu and Bi states remain unchanged with respect to the undistorted structure. Meanwhile, it is clearly observed in Fig. 5(i) and (j) that in the valence band, the *4s-Fe* and *3p-Fe* orbitals in the spin down channel undergo a shift away from the Fermi level, locating now between −8.09 and −8.58 eV, while in the conduction band the *3d-Fe* states in the spin down channel are responsible for an increase of 1.10 eV in the band gap value, presenting a significant shift towards the higher energy regime. Although slight variations in the *3d-Fe* and *2p-O* states are observed for the spin configuration, there are no significant changes in the energy location of these orbitals. Similarly, strong hybridizations between their orbitals remain for the two turning orientations.

Comparative results between the density of states without and with Berry phase reveal no significant changes in the contributions of the Bismuth electronic states for the two spin orientations, both in the valence band and in the conduction band. On the other hand, when applying the Berry phase, an increase of the DOS by about 25% is observed for 4s-Fe and 3p-Fe states with the 2p-O in the valence band, far from the Fermi level, with the appearance of hybridizations between these states and the *2p-O* in the −8.58 eV < E < −8.09 eV energy regime. Similarly, in the valence band, Berry distortion produces uniformity in the hybridization of *3d-Fe* states with *2p-O* states available in the conduction band near the Fermi level for the two spin polarisations. It is circumstantially relevant to mention that Berry's phase causes a decrease of about 30% in the total DOS for the spin-up orientation, in the valence band very close to the Fermi level, due to changes in the *3d-Fe* orbitals. Similarly, it is noticeable that the bandgap values increase, becoming approximately equal for the two spin polarisations, since before the distortion the bandgap was significantly lower for the spin-down polarisation. This bandgap shift towards the higher energy regime in the conduction band is mostly due to the *3d-Fe* states, which is directly related to the structural distortion in the *Fe-O_6* octahedra.

To establish the eventual occurrence of a phase transition leading to a state of effective electrical polarization at low temperatures, calculations of thermophysical properties were carried out under the application of hydrostatic pressures up to 18 GPa in the absence and presence of the Berry phase. Fig. 6(a) and (b) show isobaric curves of the entropy difference (ΔS) and specific heat (ΔC_p) difference as a function of temperature, respectively. The differences mentioned refer to the inclusion or absence of the Berry phase. In Fig. 6(a), a

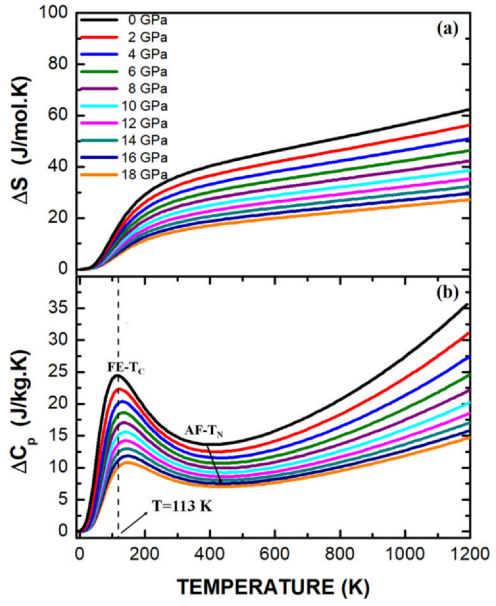

Fig. 6. ΔS (a) and specific heat ΔC_p (b) obtained by calculating the differences in entropy and specific heat with and without the Berry phase as a function of temperature under the application of several hydrostatic pressures.

pronounced change in ΔS(T) is evident at low temperatures, with a strong decrease in its absolute value with increasing applied pressure. In Fig. 6(a), a pronounced change in ΔS(T) at low temperatures is evident, with a strong tendency to adopt linear behavior at high temperatures.

With increasing applied pressure, the slope of ΔS(T) at high temperatures decreases, and a dramatic drop in its absolute value is observed, although the change at low temperatures remains abrupt. Apparently, the increase in the applied pressure favors the transit of the system towards a state with some type of greater ordering, as will be discussed later. According to the characteristics of the ΔC_p curves in Fig. 6(b), a phase transition takes place at low temperatures, approximately T = 113 K, in the absence of hydrostatic pressure. As interpreted from the experimental results [19], this would be a transition between paraelectric states (at T > 113 K) and ferroelectric states (at T < 113 K), caused by a structural transition between the centrosymmetric space group Pnma and the polar group (no centrosymmetric) I4/mcm, which is characteristic of some perovskite materials that polarize in this space group at low temperatures [43].

As shown in Fig. 7, the increase in the applied pressure shifts the Curie temperature (FE-T_C) of the formation of electric dipoles towards the higher temperature regimes. This improvement in ferroelectricity as a consequence of pressure would be because the pressure would reduce the overlap between the Fe-*3d*(e_g) and O-*2p* orbitals in the Fe-O_6 octahedra of the material, as expected for any insulating perovskite, similar to other structures that involve a transition metal surrounded by oxygen [44,45]. This decrease can be observed in the densities of partial states calculated for Fe and O presented in Fig. 5(d) and (e), without the Berry phase, in contrast to figures f(i) and 5(j) with the Berry phase.

Meanwhile, it should not be forgotten that the material exhibits magnetic ordering at high temperatures, which probably occurs for a temperature value of approximately 400 K, which is where ΔC_p, in Fig. 6(b), exhibits a strong curvature. As was initially established, the most favorable energetic ordering corresponds to the type-G antiferromagnetism, so that this transition temperature would correspond to the Néel temperature (AF-T_N), which is also affected by the increase in the applied pressure. This behavior is expected in multiferroic materials, where pressure can induce changes in the ferroelectric response [46] and can even give rise to magnetoelectrical coupling effects [47]. It is not ruled out that eventual magnetoelectric coupling takes place at T = 113 K, which can be induced by Dzyaloshinskii-Moriya interactions [48] associated with characteristic canted magnetic moments in perovskite-type antiferromagnetic materials. As discussed above (Fig. 2), the tilt introduced by the ϕ_e angle produces an Fe–O–Fe bond angle of less than 180°. In the material under study, the antiferromagnetic character can be idealised as the occurrence of antiparallel spins in the Fe cations of the FeO_6 octahedra, in which the canting in the magnetic moments, introduced by the octahedral distortions, gives rise to a weak ferromagnetic component, as expected in the Dzyaloshinskii-Moriya interaction [49]. These mechanisms would be supported by hybridizations between the 3d-Fe and 2p-O orbitals, as discussed above from the results of DOS calculations. This coupling would be favored by antisymmetric spin coupling contributions due to the combined effects of exchange and spin-orbit interactions. Thus, antiferromagnetism and ferroelectric response would coexist as a result of competition between exchange and Dzyaloshinskii-Moriya interactions, strongly influenced by frustration [50]. However, weak ferromagnetism, such as that observed experimentally in $Eu_2Bi_2Fe_4O_{12}$ [19], may appear as a consequence of changes in the Dzyaloshinskii-Moriya interaction [10].

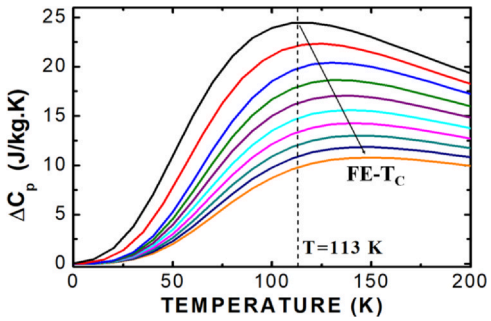

Fig. 7. Observation of the increase in ferroelectric Curie temperature with the increase in applied pressure.

4. Conclusions

The structural and electronic properties of the $Eu_2Bi_2Fe_4O_{12}$ perovskite material have been theoretically studied. Calculations were performed considering the structural Pnma space group reported from the experimental results. The energy minimization procedures suggest that the most stable ionic arrangement corresponds to an alternate distribution of Eu^{3+} and Bi^{3+} cations along the three crystallographic axes, forming a superstructure with cationic ordering. Likewise, the octahedral distortion that characterizes this family of ceramics affects the properties of the material. The results of the calculations reveal that the rotation and inclination angles of the FeO_6 octahedra that energetically stabilize the structure are $\theta_e = 12.86°$ and $\phi_e = 13.32°$, respectively. Calculations of different types of magnetic ordering for the Fe^{3+} ions throughout the structure reveal that the most likely distribution is that of a G-type antiferromagnetic material, in which the spins of the respective nearest neighbouring octahedra are always opposite. The results of density of states calculations reveal the occurrence of semiconductor-type behavior with a 2.4 eV bandgap, which is due to the majority contribution of *2p*-O orbitals in the valence band and to the hybridization with *4f*-Eu and *6p*-Bi orbitals. Meanwhile, the displacements of the Fe cation applied through the study of the Berry phase should promote a structural modification between the centrosymmetric space group and a type of polar cell (not centrosymmetric) to promote the spontaneous formation of dipole moments. The octahedral distortions introduced by the Berry phase give rise to DM interactions that allow the coexistence of spontaneous ferroelectric electric polarisation and ferromagnetic response due to canting effects in the antiferromagnetically ordered spins. Thus, a marked increase in the value of the forbidden band is obtained when the density of states is determined considering the Berry phase. The macroscopic polarization of the material was calculated through Berry's phase with a result that is consistent with the experimental results, since the behavior has a ferroelectric feature. The difference in entropy and specific heat between the states with the Berry phase and without the Berry phase (in the absence of external pressure) suggests the occurrence of a transition at T = 113 K, in agreement with the reported experimental observations. With increased hydrostatic pressure, a consequent increment in the value of this transition temperature is seen, improving the ferroelectric properties of the material. The results show that the inclusion of the Berry phase in the calculation of the density of states and in the thermodynamic properties constitutes an excellent complement to the theory in the study of the physical properties of new materials.

CRediT authorship contribution statement

A.V. Gil Rebaza: He was responsible for writing the code as part of the direction of **H.H. Medina Chanduví's** doctoral thesis. **H.H. Medina Chanduví:** Ph.D. student who participated in the calculation of the density of electronic states. **C.E. Deluque Toro:** He oversaw energy minimisation to establish the right magnetic configuration

for the calculation. **D.A. Landínez Téllez:** He participated in the interpretation of results. **J. Roa-Rojas:** Responsible for project management, interpretation of results and drafting of the manuscript.

Declaration of Competing Interest

The authors declare that they have no known competing financial interests or personal relationships that could have appeared to influence the work reported in this paper.

Acknowledgements

This work was partially supported by the Division of Investigation and Extension (DIEB) of the National University of Colombia, Fonciencias of the Universidad del Magdalena and Minciencias, on project FP80740-243-2019.

References

[1] A.S. Bhalla, R. Guo, R. Roy, The perovskite structure – a review of its role in ceramic science and technology, Mater. Res. Innov. 4 (2000) 3–26, https://doi.org/10.1007/s100190000062

[2] L. Alff, Ferrimagnetic double perovskites as spintronic materials, in: K. Scharnberg, S. Kruchinin (Eds.), Electron Correlation in New Materials and Nanosystems, NATO Science Series, 241 Springer, Dordrecht, 2007, https://doi.org/10.1007/978-1-4020-5659-8_31

[3] S. Jiang, T. Hu, J. Gild, N. Zhou, J. Nie, M. Qin, T. Harrington, K. Vecchio, J. Luo, A new class of high-entropy perovskite oxides, Scr. Mater. 142 (2018) 116–120, https://doi.org/10.1016/j.scriptamat.2017.08.040

[4] A.S. Cavichini, M.T. Orlando, J.B. Depianti, J.L. Passamai Jr., F. Damay, F. Porcher, E. Granado, Exotic magnetism and spin-orbit-assisted Mott insulating state in a 3d-5d double perovskite, Phys. Rev. B 97 (2018) 054431, https://doi.org/10.1103/PhysRevB.97.054431

[5] P. Royen, K. Swars, Das system Wismutoxyd-Eisenoxyd im Bereich von 0 bis 55 mol% Eisenoxyd, Angew. Chem. 24 (1957) 779, https://doi.org/10.1002/ange.19570692407

[6] C. Michel, J.-M. Moreau, G.D. Achenbach, R. Gerson, W.J. James, The atomic structure of $BiFeO_3$, Sol. Stat. Commun. 7 (1969) 701–704, https://doi.org/10.1016/0038-1098(69)90597-3

[7] F. Kubel, H. Schmid, Structure of a ferroelectric and ferroelastic monodomain crystal of the perovskite $BiFeO_3$, Acta Cryst. B 46 (1990) 698–702, https://doi.org/10.1107/S0108768190006887

[8] A.M. Kadomtseva, Y.F. Popor, A.P. Pyatakov, G.P. Vordolev, A.K. Zvezdin, D. Viehland, Phase transitions in multiferroic $BiFeO_3$ crystals, thin-layers, and ceramics: enduring potential for a single phase, room-temperature magnetoelectric 'holy grail', Phase Transit. 79 (2006) 1019–1042, https://doi.org/10.1080/01411590601067235

[9] A. Reyes, C. de la Vega, Ma.E. Fuentes, L. Fuentes, $BiFeO_3$: synchrotron radiation structure refinement and magnetoelectric geometry, J. Eur. Ceram. Soc. 27 (2007) 3709–3711, https://doi.org/10.1016/j.jeurceramsoc.2007.02.034

[10] C. Ederer, N.A. Spaldin, Weak ferromagnetism and magnetoelectric coupling in bismuth ferrite, Phys. Rev. B 71 (2005) 060401, https://doi.org/10.1103/PhysRevB.71.060401

[11] J. Wang, J.B. Neaton, H. Zheng, V. Nagarajan, S.B. Ogale, B. Liu, D. Viehland, V. Vaithyanathan, D.G. Scholm, U.V. Waghmare, N.A. Spaldin, K.M. Rabe, M. Wuttig, R. Ramesh, Epitaxial $BiFeO_3$ multiferroic thin film heterostructures, Science 299 (2003) 1719–1722, https://doi.org/10.1126/science.1080615

[12] M. Eibschütz, Lattice constants of orthoferrites, Acta Cryst. 19 (1965) 337–339, https://doi.org/10.1107/S0365110×65003419

[13] M.K. Warshi, V. Mishra, A. Sagdeo, V. Mishra, R. Kumar, P.R. Sagdeo, Synthesis and characterization of $RFeO_3$: experimental results and theoretical prediction, J. Mater. Process. Technol. 4 (2018) 558–572, https://doi.org/10.1080/2374068X.2018.1483680

[14] Z.-Q. Wang, Y.-S. Lan, Z.-Y. Zeng, X.-R. Chen, Q.-F. Chen, Magnetic structures and optical properties of rare-earth orthoferrites $RFeO_3$ (R = Ho, Er, Tm and Lu), Sol. Stat. Commun. 288 (2019) 10–17, https://doi.org/10.1016/j.ssc.2018.11.004

[15] K. Sultan, M. Ikram, K. Asokan, Effect of Mn doping on structural, morphological and dielectric properties of $EuFeO_3$ ceramics, RSC Adv. 5 (2015) 93867–93876, https://doi.org/10.1039/C5RA20514J

[16] D. Treves, Studies on orthoferrites at the Weizmann Institute of Science, J. Appl. Phys. 36 (1965) 1033–1039, https://doi.org/10.1063/1.1714088

[17] W.M. Xu, M.P. Pasternak, G.K. Rozenberg, R.D. Taylor, Pressure-induced spin-crossover in $EuFeO_3$, Hyperfine Interact. 141/142 (2002) 243–247, https://doi.org/10.1023/A:1021243128644

[18] I.H. Lone, J. Aslam, N.R.E. Radwan, A.H. Bashal, A.F.A. Ajlouni, A. Akhter, Multiferroic ABO_3 transition metal oxides: a rare interaction of ferroelectricity and magnetism, Nanoscale Res. Lett. 14 (2019) 142, https://doi.org/10.1186/s11671-019-2961-7

[19] J.A. Cuervo-Farfán, C.A. Parra Vargas, D.S.F. Viana, F.P. Milton, D. Garcia, D.A. Landínez Téllez, J. Roa-Rojas, Structural, magnetic, dielectric and optical properties of the $Eu_2Bi_2Fe_4O_{12}$ bismuth-based low-temperature biferroic, J. Mater. Sci. Mater. Electron. 29 (2018) 20942–20951, https://doi.org/10.1007/s10854-018-0238-z

[20] J.A. Cuervo Farfán, D.M. Aljure García, R. Cardona, J. Arbey Rodríguez, D.A. Landínez Téllez, J. Roa-Rojas, Structure, ferromagnetic, dielectric and electronic features of the $LaBiFe_2O_6$ material, J. Low Temp. Phys. 186 (2017) 295–315, https://doi.org/10.1007/s10909-016-1714-6

[21] E. Vasala, M. Karppinen, $A_2B'B''O_6$ perovskites: a review, Prog. Sol. State Phys. 43 (2015) 1–36, https://doi.org/10.1016/j.progsolidstchem.2014.08.001

[22] P.M. Woodward, Octahedral tilting in perovskites. II. Structure stabilizing forces, Acta Cryst. B 53 (1997) 44–66, https://doi.org/10.1107/S0108768196012050

[23] C.J. Howard, B.J. Kennedy, P.M. Woodward, Ordered double perovskites – a group-theoretical analysis, Acta Cryst. B 59 (2003) 463–471, https://doi.org/10.1107/S0108768103010073

[24] R. Resta, Macroscopic polarization in crystalline dielectrics: the geometric phase approach, Rev. Mod. Phys. 66 (1994) 899–915, https://doi.org/10.1103/RevModPhys.66.899

[25] R. Resta, Polarization as a Berry phase, Europhysics News, 28 (1997), pp. 18–20, https://doi.org/10.1007/s00770-997-0018-4

[26] C.E. Deluque Toro, A.S. Mosquera Polo, A.V. Gil Rebaza, D.A. Landínez Téllez, J. Roa-Rojas, Ab Initio study of the electronic structure, elastic properties, magnetic feature and thermodynamic properties of the Ba_2NiMoO_6 material, J. Low Temp. Phys. 192 (2018) 265–285, https://doi.org/10.1007/s10909-018-1937-9

[27] C.E. Alarcón-Suesca, C.E. Deluque Toro, A.V. Gil Rebaza, D.A. Landínez Téllez, J. Roa-Rojas, Ab-initio studies of electronic, structural and thermophysical properties of the Sr_2TiMoO_6 double perovskite, J. Alloy. Compd. 771 (2019) 1080–1089, https://doi.org/10.1016/j.jallcom.2018.08.314

[28] M.A. Blanco, A.M. Pendás, E. Francisco, J.M. Recio, R. Franco, Thermodynamical properties of solids from microscopic theory: applications to MgF_2 and Al_2O_3, J. Mol. Struct. Theochem 368 (1996) 245–255, https://doi.org/10.1016/S0166-1280(96)90571-0

[29] R. Martin, Electronic Structure: Basic Theory and Practical Methods, Cambridge University Press, USA, 2008.

[30] P. Giannozzi, O. Andreussi, T. Brumme, O. Bunau, M.B. Nardelli, M. Calandra, R. Car, C. Cavazzoni, D. Ceresoli, M. Cococcioni, N. Colonna, I. Carnimeo, A.D. Corso, S. de Gironcoli, P. Delugas, R.D. Jr, A. Ferretti, A. Floris, G. Fratesi, G. Fugallo, R. Gebauer, U. Gerstmann, F. Giustino, T. Gorni, J. Jia, M. Kawamura, H.-Y. Ko, A. Kokalj, E. Kkbenli, M. Lazzeri, M. Marsili, N. Marzari, F. Mauri, N. Nguyen, H.-V. Nguyen, A.O. de-la Roza, L. Paulatto, S. Ponc, D. Rocca, R. Sabatini, B. Santra, M. Schlipf, A. Seitsonen, A. Smogunov, I. Timrov, T. Thonhauser, P. Umari, N. Vast, X. Wu, S. Baroni, Advanced capabilities for materials modelling with Quantum Espresso, J. Phys. Condens Matter 29 (2017) 465901, https://doi.org/10.1088/1361-648X/aa8f79

[31] J. Perdew, K. Burke, M. Ernzerhof, Generalized gradient approximation made simple, Phys. Rev. Lett. 78 (1997) 1396, https://doi.org/10.1103/PhysRevLett.78.1396

[32] I. Timrov, N. Marzari, M. Cococcioni, Hubbard parameters from density-functional perturbation theory, Phys. Rev. B B 98 (2018) 085127, https://doi.org/10.1103/PhysRevB.98.085127

[33] M. Cococcioni, S. De Gironcoli, Linear response approach to the calculation of the effective interaction parameters in the LDA + U method, Phys. Rev. B 71 (2005) 035105, https://doi.org/10.1103/PhysRevB.71.035105

[34] G. Prandini, A. Marrazzo, I. Castelli, N. Mounet, N. Marzari, Precision and efficiency in solid-state pseudopotential calculations, npj Comput. Mater. 4 (2018) 72, https://doi.org/10.1038/s41524-018-0127-2

[35] H.J. Monkhorst, J.D. Pack, Special points for Brillouin-zone integrations, Phys. Rev. B 13 (1976) 5188–5192, https://doi.org/10.1103/PhysRevB.13.5188

[36] R.D. King-Smmith, D. Vanderbilt, Theory of polarization of crystalline solids, Phys. Rev. B 47 (1993) 1651–1654, https://doi.org/10.1103/PhysRevB.47.1651

[37] D. Vanderbilt, Berry-phase theory of proper piezoelectric response, J. Phys. Chem. Solid. 61 (2000) 147–151, https://doi.org/10.1016/S0022-3697(99)00273-5

[38] R. Resta, M. Posternak, A. Baldereschi, Towards a quantum theory of polarization in ferroelectrics: the case of $KNbO_3$, Phys. Rev. Lett. 70 (1993) 1010–1013, https://doi.org/10.1103/PhysRevLett.70.1010

[39] C.E. Deluque-Toro, D.A. Landínez-Téllez, J. Roa-Rojas, Ab-initio analysis of magnetic, structural, electronic and thermodynamic properties of the Ba_2TiMnO_6 manganite, DYNA 85 (2018) 27–36, https://doi.org/10.15446/dyna.v85n205.68517

[40] J.A. Cuervo Farfán, C.E. Deluque Toro, C.A. Parra Vargas, D.A. Landínez Téllez, J. Roa-Rojas, Experimental and theoretical determination of physical properties of $Sm_2Bi_2Fe_4O_{12}$ ferromagnetic semiconductors, J. Mater. Chem. C 8 (2020) 14925–14938, https://doi.org/10.1039/d0tc02935a

[41] A.M. Glazer, Simple ways of determining perovskite structures, Acta Crystallogr. A 31 (1975) 756–762, https://doi.org/10.1107/S0567739475001635

[42] B.D. Cullity, C.D. Graham, Introduction to Magnetic Materials, second ed., IEEE Press and John Wiley and Sons, Inc.,, 2009.

[43] S.K. Mishra, D. Pandey, Low temperature x-ray diffraction study of the phase transitions in $Sr_{1-x}Ca_xTiO_3$ (x = 0.02,0.04): evidence for ferrielectric ordering, Appl. Phys. Lett. 95 (2009) 232910, https://doi.org/10.1063/1.3273863

[44] I.A. Kornev, L. Bellaiche, P. Bouvier, P.-E. Janolin, B. Dkhil, J. Kreisel, Ferroelectricity of Perovskites under pressure, Phys. Rev. Lett. 95 (2005) 196804, https://doi.org/10.1103/PhysRevLett.95.196804

[45] I.A. Kornev, L. Bellaiche, The nature of ferroelectricity under pressure, Phase Transit. 80 (2007) 385–413, https://doi.org/10.1080/01411590701228117
[46] L.J. Ding, Y. Zhong, A theoretical strategy for pressure-driven ferroelectric transition associated with critical behavior and magnetoelectric coupling in organic multiferroics, Phys. Chem. Chem. Phys. 22 (2020) 19120–19130, https://doi.org/10.1039/D0CP03003A
[47] E. Gilioli, L. Ehm, High pressure and multiferroics materials: a happy marriage, IUCrJ 1 (2014) 590–603, https://doi.org/10.1107/S2052252514020569
[48] F.K. Fodouop, G.C. Fouolceng, M. Tchoffo, L.C. Fai, N. Randrianantoandro, Thermodynamics of metamagnetoelectric effect in multiferroics, J. Magn. Magn. Mater. 474 (2019) 456–461, https://doi.org/10.1016/j.jmmm.2018.10.080
[49] S. Dong, H. Xiang, E. Dagotto, Magnetoelectricity in multiferroics: a theoretical perspective, Natl. Sci. Rev. 6 (2019) 629–641, https://doi.org/10.1093/nsr/nwz023
[50] I.A. Sergienko, E. Dagotto, Role of the Dzyaloshinskii-Moriya interaction in multiferroic perovskites, Phys. Rev. B 73 (2006) 094434, https://doi.org/10.1103/PhysRevB.73.094434